Biosensors based on Si_3N_4 Asymmetric Mach-Zehnder Interferometers

Tatevik Chalyan[a,*], Laura Pasquardini[b,†], Floris H. Falke[c], Manuela Zaneti[b], Romain Guider[a], Davide Gandolfi[a], Erik Schreuder[c], Cecillia Pederzolli[b], Rene G. Heideman[c], and Lorenzo Pavesi[a]

[a]Nanoscience Laboratory, Department of Physics, University of Trento, Via Sommarive 14, 38123 Povo (TN), Italy
[b]LaBSSAH, Fondazione Bruno Kessler, Via Sommarive 18, 38123 Povo (TN), Italy
[c]LioniX B.V., PO Box 456, 7500 AL Enschede, The Netherlands

ABSTRACT

In this work, we present a study on photonic biosensors based on Si_3N_4 asymmetric Mach-Zehnder Interferometers (aMZI) for Aflatoxin M1 (AFM1) detection. AFM1 is an hepatotoxic and a carcinogenic toxin present in milk. The biosensor is based on an array of four Si_3N_4 aMZI that are optimized for 850nm wavelength. We measure the bulk Sensitivity (S) and the Limit of Detection (LOD) of our devices. In the array, three devices are exposed and have very similar sensitivities. The fourth aMZI, which is covered by SiO_2, is used as an internal reference for laser (a VCSEL) and temperature fluctuations. We measured a phase sensitivity of 14300±400 rad/RIU. To characterize the LOD of the sensors, we measure the uncertainty of the experimental readout system. From the measurements on three aMZI, we observe the same value of LOD, which is $\approx 4.5\times10^{-7}$ RIU. After the sensor characterization on homogeneous sensing, we test the surface sensing performances by flowing specific Aflatoxin M1 and non-specific Ochratoxin in 50 mM MES pH 6.6 buffer on the top of the sensors functionalized with Antigen-Recognising Fragments (Fab'). The difference between specific and non-specific signals shows the specificity of our sensors. A moderate regeneration of the sensors is obtained by using glycine solution.

Keywords: asymmetric Mach-Zehnder Interferometers, Aflatoxin M1, sensitivity, Limit of Detection, Antigen-Recognising Fragments

1. INTRODUCTION

The first optical sensors came into sight starting in 1937, when Langmuir and Schaefer described the determination of a biomolecule adlayer thickness formed on a metallic surface via the observation of colors produced by reflective interference.[1] The real outbreak of optical biosensors happened in the mid-90s with development and realization of microfabrication technologies and detection systems.[2] Since then optical biosensors, and in particular label-free optical biosensors, have become one of the most active and attractive fields within the biosensing devices. The preference on optical label-free biosensors is mainly attributed to a number of unique characteristics such as the use of light, which removes electrical interferences and the excellent bioanalytical performance in terms of limit of detection (LOD) and sensitivity (S). In addition, the easy fabrication with standard microelectronic/micromachining processes guarantees low cost and mass production. Systems for a wide range of applications which include human health, food safety and environmental monitoring have been proposed.

Although Surface Plasmon Resonance (SPR) based sensors have found commercial applications,[3] integrated optical sensors have shown very promising results. In particular, devices like ring resonators[4] and MachZehnder interferometers[5] are showing high sensitivities and miniaturization abilities, which allow the realization of an integrated lab-on-chip device.[6–8]

Further author information: (Send correspondence to T.C)
*T.C.: E-mail: tatevik.chalyan@unitn.it, Telephone: (+39) 3898975929
†Present address: Department of Industrial Engineering, University of Trento, Via Sommarive 9, 38123 Povo (TN), Italy

For diary applications we are interested in a biosensor for a fast and comprehensive detection of Aflatoxin M1 (AFM1) mycotoxin.[5,6] AFM1 is a milk contaminant and a potent carcinogen substance, regulated by the European Commission (EC No. 1881/2006). At present, the level of AFM1 in milk is analyzed using screening tests like Enzyme-Linked ImmunoSorbent Assay (ELISA). In addition, High-Performance Liquid Chromatography is needed when samples show suspect concentration of AFM1. The combination of these analyses is expensive, time-consuming and bulky.

The optical biosensor which we are here proposing is based on an asymmetric Mach-Zehnder Interferometer (aMZI), with silicon nitride (Si_3N_4) as core material and silica (SiO_2) as cladding material. They are fabricated by standard CMOS processing and can be assembled with fluidics in a compact package. The basic idea behind the sensor is that the interference at the output of an aMZI is affected by the phase difference between the light which travels along the two interferometer arms. By opening a window in the SiO_2 and exposing one of the two arms to an analyte, the change in the refractive index in the window region is measured as an interference fringe shift in the aMZI output signal. From the fringe shift, the phase shift suffered by the light that travels in the exposed arm can be determined. From the phase shift, the change of the refractive index is measured, i.e., the sensor can sense the analyte.

The Mach-Zehnder interferometer is made asymmetric by the addition of a small path length difference between both arms and by the difference of refractive index between the liquid and SiO_2 which cover the two arms. This difference results in a wavelength dependency of the output phase. Scanning the aMZI over a small laser wavelength bandwidth results in a phase measurement by the phase shift, due to a refractive index change, can be monitored with high accuracy.

One of the most important characteristic for a biosensor is the specificity. In order to develop a biosensor specific to the detection of AFM1, a functionalization process based on antigen-binding fragments (Fab') was applied on the aMZI surface. One benefit of using antibodies is the extreme specificity associated with their antigen-binding site.[9] The immobilization of antibodies includes whole antibodies, F(ab')2, and Fab' fragments. Antibodies need to be immobilized in a controlled and oriented fashion, in order to maximize the number of available antigen-binding sites. Although significant progress has been made with whole antibody immobilization, methods for the immobilization of Fab' fragments have become relevant especially for biosensor development,[10–12] offering several benefits over whole antibodies. Firstly, bound Fab' fragments are able to maintain a higher amount of binding sites per unit area compared to whole antibodies due to their smaller size. Moreover, Fab fragments are immobilized easily in an oriented conformation via the nucleophilic sulde near their C-terminals.

In this work, we measured and analyzed the selectivity and regeneration of functionalized asymmetric Mach-Zehnder interferometric biosensors with purified solutions. First, we describe the experimental setup and the functionalization procedure of the sensor. Then, we performed sensing measurements using two mycotoxins, AFM1 and Ochratoxin (OTA), in buffer solution for various concentrations, and, finally, we performed regeneration measurements using glycine solutions.

2. EXPERIMENTAL SECTION

2.1 Materials

3-mercaptopropyltrimethoxysilane (MPTMS, 99%) purchased from Gelest Ltd. (Maidstone, Kent, UK), was used without any further purification. Toluene anhydrous (99.8%), toluene, dithiothreitol (DTT) and all powders for buffered solutions were purchased from Sigma-Aldrich s.r.l. (Milan, Italy). Methoxypolyethyleneglycolthiol (mPEG-SH) with 2000 and 5000 molecular weights were purchased from Nektar Therapeutics AL (Huntsville, AL, USA). A rabbit polyclonal anti-AFM1 antibody and a horseradish peroxidase (HRP)-conjugated Aflatoxin M1 (AFM1-HRP) contained in the Iscreen Afla M1 milk Elisa kit were purchased from Tecna s.r.l. (Padua, Italy), while Aflatoxin M1 and Ochratoxin were purchased from Sigma-Aldrich s.r.l. (Milan, Italy). SuperSignal West Femto Chemiluminescent Substrate was purchased from Thermo Scientific (Rockford, IL, USA).

2.2 Functionalization Process

F(ab')$_2$ fragments are generated by protease digestion (Immobilized Papain Thermo Scientific) of 20 μL of 1 mg/mL anti-AFM1 polyclonal rabbit IgG according to manufacturer's instructions. Then, a 13.3 μM F(ab')$_2$ solution is mixed with 10 mM DTT to reduce the disulphide bond in the hinge region, and the mixture is incubated for two hours at room temperature. The mixture is poured into a centrifugal filter unit (Microcon YM-10, MWCO 10000, Millipore Corp., Billerica, MA, USA) to remove the excess of DTT.[6] The Fab' are immobilized on the Si_3N_4 surface adapting the protocol described in Yoshimoto et al.,[13] with some modifications. In order to introduce thiol groups able to react with the cysteine groups on Fab' fragments, the silicon nitride surface is functionalized in wet conditions with mercaptosilane (MPTMS). The aMZI surface is cleaned with an argon plasma (6.8 W, one min) to remove organic contaminants and to hydroxylate the surface and is then immersed in a 1% v/v solution of MPTMS in toluene anhydrous at 60 $^{\circ}C$ for 10 min. Silane-coated chips are rinsed several times with toluene and then dried in a stream of nitrogen. The immobilization of Fab' fragments onto the surface is carried out by deposition of 80 μL of a 0.33 μM Fab' in 10 mM phosphate buffer with 10 mM ethylenediaminetetraacetic acid (EDTA). After two minutes, the surface is PEGylated by addition first of 200 μM final concentration of mPEG-SH 5000 (for 30 min on orbital shaker at 80 rpm) and then of 200 μM of mPEG-SH 2000 (for 60 min on shaker at 80 rpm). An additional step based on casein passivation is added. The functionalized chip is exposed at 0.1mg/ml of casein solution for 30 minutes, in order to increase the chip performances in a slightly dirty solution. The surface is finally cleaned using a PBS-EDTA buffer. The concentration of the Fab' is determined by measuring their absorbance with a Nanodrop instrument (Extinction coefficient (0.1%) = 1.35 at 280 nm).

2.3 Mach-Zehnder Interferometers: Fabrication Process and Design

The aMZI devices are based on the TriPlex technology.[10] A 4 inches 525 μm thick silicon substrate is oxidized until 8 μm thermal oxide layer is formed on the surface. Then, a single 103 nm thick LPCVD (low-pressure chemical vapor deposition) Si_3N_4 layer (refractive index 2.02) is deposited onto the thermal oxide followed by a thin LPCVD SiO_2 layer. This layer stack is patterned by using photolithography, dry etching (RIE) and subsequently resist removal. The waveguides are then covered with a thick 6 μm LPCVD SiO_2 cladding. To enable the interaction between the evanescent field of the light propagating through the waveguide and the liquid sample of interest, the top cladding is locally removed by opening the sensing window. This is accomplished by a photolithography step and BHF wet etch down to the Si_3N_4 layer.[8] An image of the sensor is reported in Fig. 1. Four aMZI are integrated in a single chip. A same input signal is sent to the four aMZI by a one to four channel splitter. The long optical path length of the sensing arms is 6.25 mm, and it is achieved by a spiral waveguide to minimize the footprint.The difference in optical path-length determines the free spectral range (FSR) of the aMZI and is chosen such that it matched with the bandwidth of the used Vertical-Cavity Surface-Emitting Laser (VCSEL). Three out of the four aMZI have the sensing window on top of the sensing arm. Openings are shown in the Fig.1 by blue hatched regions. The fourth aMZI is left covered by the cladding in order to isolate it from the microfluidic chamber and, therefore, to be used as the reference sensor (baseline sensor). This aMZI is used as an internal reference both for the input signal intensity (e.g. to control the VCSEL fluctuations) and for temperature. The area of and pitch between the sensors are chosen such that each individual sensor can be functionalized by a spotter with a different chemistry allowing internal consistency tests or multianalyte detection. Note that the input and output waveguides are all on the same edge of the chip.

2.4 Theoretical Background

The basic concept of interferometry is to split a beam of light into two separate paths and then to look at their interference in order to measure the phase delay due to a different optical path length. Therefore, aMZI can be used to detect the phase delay caused by the light interaction with the sensing liquid.[11] A change in the refractive index of the sensing liquid affects the effective index experienced by the light in the waveguides, n_{eff}, and this, in turn, affects the phase shift. Let us assume that the two arms of the aMZI have lengths L_A and L_B, and effective indexes $n_{eff,A}$ and $n_{eff,B}$, respectively. The two arms of the interferometer are intentionally unbalanced, so that the transmission at the output port is wavelength-dependent also when the two effective indexes are equal. Let us call A the exposed arm. Moreover, let us assume that the wavelength scan is performed

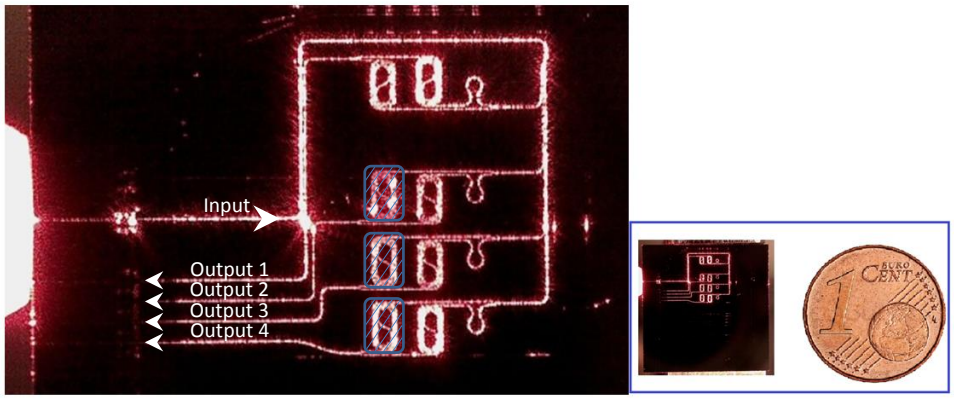

Figure 1. Photograph of the asymmetric MachZehnder interferometer chip; (inset) photograph of the chip and a one euro-cent coin for size comparison.

in a small range ($\delta\lambda$) starting from a given wavelength (λ_0), then the phase difference accumulated by the light during the propagation in the two arms ($\Phi(\lambda)$) is

$$\Phi(\lambda) = \Phi(\lambda_0 + \delta\lambda) \approx \frac{2\pi}{\lambda_0}(n_{eff,A}L_A - n_{eff,B}L_B)(1 - \frac{\delta\lambda}{\lambda_0}) = \Phi_0 - \frac{2\pi\delta\lambda}{\lambda_0^2}(n_{eff,A}L_A - n_{eff,B}L_B)\,, \tag{1}$$

where

$$\Phi_0 = \frac{2\pi}{\lambda_0}(n_{eff,A}L_A - n_{effB}, L_B)\,, \tag{2}$$

By defining $\Lambda = {\lambda_0}^2/(\mathrm{n}_{eff,A}\mathrm{L}_A\text{-}\mathrm{n}_{eff,B}\mathrm{L}_B)$, we can straightforwardly compute the transmission spectrum of the aMZI as

$$T(\lambda_0 + \delta\lambda) \approx \frac{1}{2}[1 + \cos(\Phi_0 - \frac{2\pi\delta\lambda}{\Lambda})]\,. \tag{3}$$

Here we note that Λ plays the role of a Free Spectral Range (FSR) of the aMZI. Note that Λ can be made arbitrarily short by increasing the optical path difference between the two arms. Reducing the FSR, the steepness of the curves of the transmission spectrum and the number of visible peaks (and valleys) in a given wavelength range increase. Therefore, Λ sets the intrinsic resolution for the measurement of the phase $\Phi(\lambda)$. $\Phi(\lambda)$ is measured via a sinusoidal fit of the transmission spectrum, and from its variation changes in the refractive index n_A are measured. The bulk sensitivity (S_b) is computed as

$$S_b = \frac{\partial\Phi_0}{\partial n_A} = \frac{2\pi L_A}{\lambda_0}\frac{\partial n_{eff,A}}{\partial n_A}\,, \tag{4}$$

Note that S_b is independent of the actual Φ_0 value, and that S_b can be increased by choosing a longer L_A. In conclusion, in the design of the aMZI we have the freedom to independently set the sensitivity and resolution of the sensor. In particular, both parameters can be enhanced by increasing L_A. However, there is a catch: in this analysis we neglected the effects of propagation losses. If the device is made too big, the absolute intensity and the visibility of the fringes at the output will decrease. This poses an ultimate limit to the achievable LOD, which represents the minimum amount of input that can be distinguished with a certain confidence level. If σ is the standard deviation of repeated measurements of blank solutions, then the LOD can be calculated as

$$LOD = \frac{k\sigma}{S_b}\,. \tag{5}$$

International Union of Pure and Applied Chemistry (IUPAC) recommends the use of k=3, which sets the confidence level to 99,7%.

2.5 Experimental Setup

The input waveguide and the four output waveguides in the chip (Fig. 1) are interfaced to a fiber array. We used a miniaturized fiber array to chip alignment setup (Fig. 2) which reliably and quickly aligns and fastens the photonic chip to the fiber array and, at the same time, provides the microfluidic circuits. A clamp mechanism presses the photonic chip into a predefined corner of a frame. This assures a first rough alignment of the chip with the fiber array with micrometric resolution. The frame where the fiber array and sensor chip are placed is milled in a single movement, ensuring a minimal alignment inaccuracy on the non adaptable pitch, roll and yaw axis. Horizontal leveling of chip to fiber array is accomplished when the cover part with integrated connectors for fluidic capillaries is pushed down onto the chip. In the same movement, a 100 μm height flow-cell is created by an integrated Viton O-ring underneath the cover part which seals off an elliptical area between the two connectors and the sensor area. Fine tuning of the alignment is then realized by maximizing the output signals with y and z movements. A ULM850-B2-PL VCSELs from Philips Technologies GmbH U-L-M Photonics connected to a single mode visible fiber is used as light source. The input signal polarization is controlled by a two-paddle polarization controller. For the detection, we connected the fibers to Si transimpedance amplified photodetectors interfaced to a PicoScope 4824 (an 8 channel USB oscilloscope). Finally, the scan in the source wavelength is achieved by current tuning of the VCSEL with a periodic current ramp which also triggers the time scan of the PicoScope. In this way, a wavelength scan of the four aMZI output waveguides is recorded by the oscilloscope and transferred to the control computer. Here the signals are processed and a live recording of the phase shifts of the signal light propagating in the four aMZI is achieved with a VCSEL modulation frequency of 20 Hz, and a data acquisition of 50,000 points per spectrum. For sensitivity and sensing measurements, we use capillaries with a diameter of 150μm, placed on the alignment stage and connected to a VICI M6 liquid handling pump.

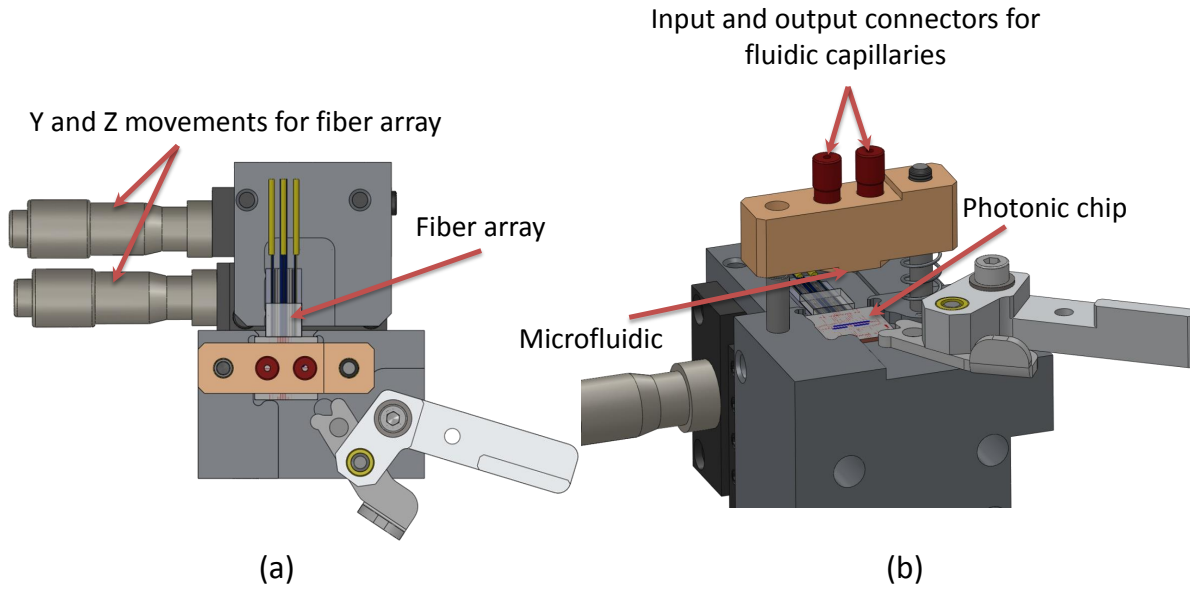

Figure 2. 3D renderings of the miniaturized alignment stage: The aMZI chip is placed into the insert of the holder and clamped into the corner by the handle. The chip is pressed downwards and leveled horizontal with the fiber array when the cover part with fluidic connectors and integrated flow-cell is pushed down. An integrated Viton O-ring assures a leak thigh connection between the photonic chip and the cover part and, at the same time, creates the flow cell over the sensor surface.

3. RESULTS AND DISCUSSIONS

3.1 Sensitivity and Limit of Detection

In order to define the performances of our photonic sensors, we characterized the volume Sensitivity (S_b) of the uncovered aMZI. To calculate this parameter, we monitored in real-time the phase shift of the aMZI, as one arm of the sensor was exposed to glucose-water solutions of various concentrations.[6] The measurement starts with flowing MES buffer, which serves as a reference liquid, then controlled quantities of glucose solutions are injected. Figure 3(a) reports the phase shifts as a function of the bulk refractive index variations measured simultaneously on the four aMZI. We note that adding the glucose-water solution causes a significant phase shift which is similar for the three sensors on the chip. One of the aMZI is covered by cladding and, consequently, the change of the flowing liquid over its surface does not lead to the phase shift. The small changes of the aMZI-1 phase monitors the fluctuations in the system: i.e. laser oscillations, temperature change. Figure 3(b) shows the dependence of the phase shift versus the refractive index of the solution, i.e. the bulk sensitivity. We found S_b = 14300±400 rad/RIU for all three exposed sensors. The LOD associated to this measurement was 1.23×10^{-6} RIU.

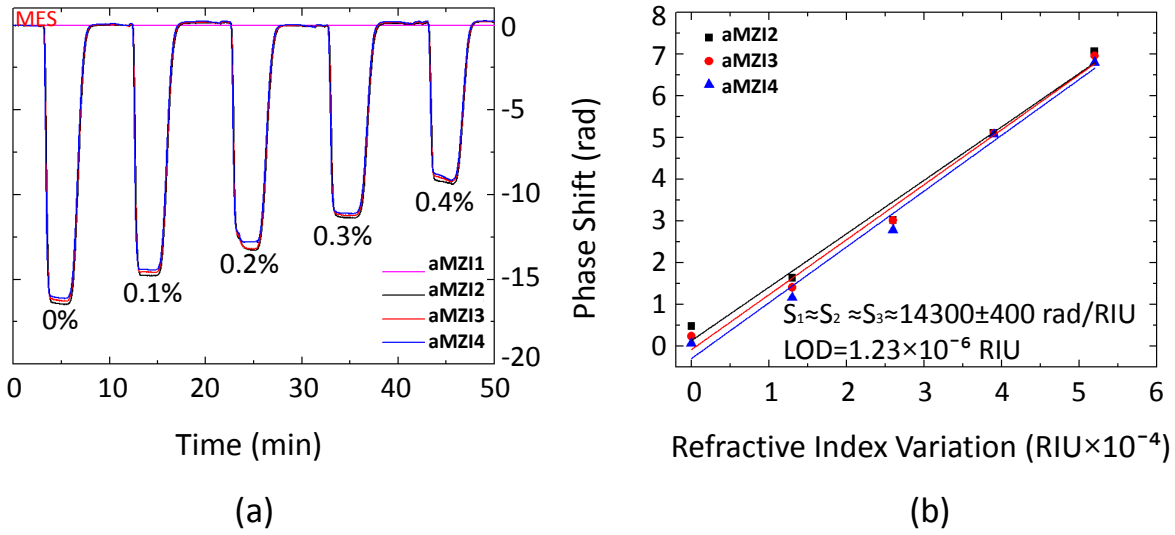

Figure 3. Bulk sensitivity measurements. (a): phase shift curves for all four aMZI sensors during the injection of the water-glucose solutions (glucose concentration in %w/w labeled on the plot). (b): Evaluation of the bulk sensitivity.

To have a statistic data for sensitivity and LOD, we repeated volumetric sensing measurements for more than 10 different photonic chips. Figure 4 represents the resulting histogram for S_b and LOD. A 3% spread of the sensitivity values is observed which is an indication of the repeatibility of the sensor fabrication and testing. The average S_b≈12650 ± 400 rad/RIU, while the average LOD ≈ $(1.1 \pm 0.2) \times 10^{-6}$ RIU value. These values for S_b and LOD show good performances of our sensors in comparison with other MZI platforms.[8,9]

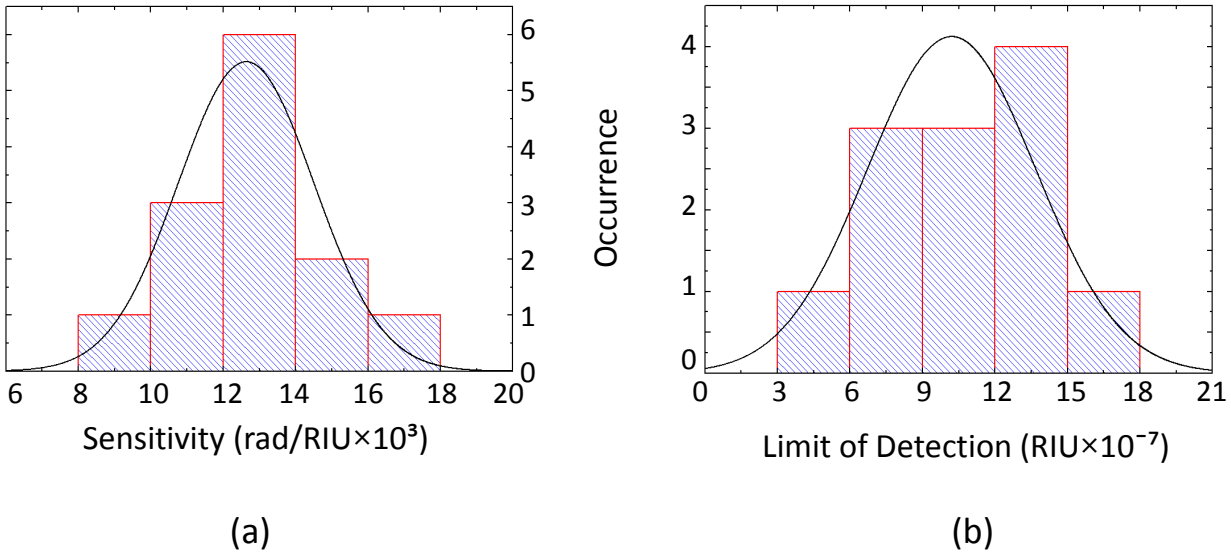

Figure 4. Statistics for the sensitivity and LOD for numerous aMZI chips. (a): Histogram for sensitivity obtained by volumetric sensing measurements. The average value is 12650±400 rad/RIU, even though the best sensitivity we achieved was 16000±1000 rad/RIU. (b): Histogram for LOD. The lowest LOD that we calculated was 4.75×10^{-7} RIU. However the average value for LOD is $(1.1 \pm 0.2) \times10^{-6}$ RIU.

3.2 Sensing Measurements

Figure 5 shows one complete measurement cycle. This includes toxin injection and regeneration of the sensors. To perform sensing measurements on these sensors, we initially filled the microfluidic chamber with a 50 mM MES buffer with pH 6.6. We then injected 50 μL of a solution containing the targeted mycotoxin (AFM1 or OTA, which is another mycotoxin of similar molecular weight) at a known concentration in order to measure the evolution of the phase of the aMZI due to the capture of the toxins from the functionalized aMZI. Note that the functionalization aims at detecting AFM1 and not OTA, so this experiment allows testing the specificity of the sensor response as well. The solution is inserted into the microfluidic chamber using an injection loop in order to avoid the formation of air bubbles in the microfluidic chamber during the buffer exchange and to have a known fixed injected volume. All measurements were done with a flow rate of 5 μL/min.

The measurement starts with flowing MES buffer over the sensors. The phase of the three exposed sensors stays constant while flowing the buffer. We consider this phase value as the phase baseline. Then, we injected a 10 nM AFM1 solution. The solution reached the sensor surfaces after 40 seconds when we observed a large phase shift and, then, the phase grew almost linearly due to the specific binding of AFM1 to the exposed surfaces of the three aMZI. It looks like the binding of the toxin occurred between 2,5 and 7,5 minutes. A subsequent flow of MES buffer caused a decrease in the phase due to the difference in bulk refractive index of solution 1 (just MES) and solution 2 (AFM1 diluted in MES). However the phase do not recover to the initial value due to the stable AFM1 binding on the surface, which is not rinsed with the subsequent flow of buffer solution. The phase shift in time follows the kinetics of the binding and dissociation of the toxin to the antibody on the surface of the exposed aMZI arms. Finally, we injected a glycine solution at the 20th minute, in order to break the Aflatoxin-antibody bonds and remove all the linked toxins from the sensor surface while keeping the antibodies in place: i.e., we aimed to regenerate the sensor. After glycine solution at the 28th minute we injected MES again and the signal recovered the baseline. This means that AFM1 were completely removed from the surfaces of the sensors.

To determine the limit of detection for AFM1, we performed measurements with different concentrations of AFM1. We compared the signals from fresh aMZI, i.e. freshly functionalized aMZI. Figure 6 shows the results for 50 nM, 10 nM and 5 nM AFM1 solutions for one aMZI. We can appreciate the clear dependence of the

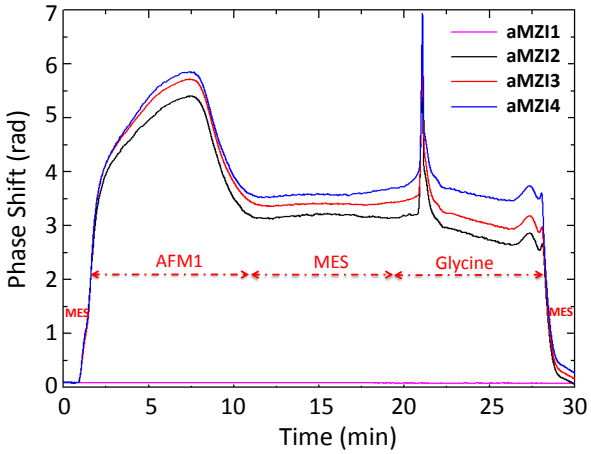

Figure 5. Sensorgram recorded on the aMZI sensors for a 10 nM AFM1 solution. At t = 0, MES buffer is flowing through the sensors. The toxin was injected at t = 30 s and at t = 7.5 min the toxin flow is stopped and the MES buffer was injected again. After 10 minutes glycine solution was injected. At t = 28 min MES buffer was injected again.

phase shift (after rinsing) on the injected toxin concentration. With decrease of the concentration we observe decrease of the phase shift proportional to the concentration changes. The biosensor was able to sense a 5 nM solution. Considering the molecular weight of AFM1 of 328.27 g/mol, 5 nM corresponds to 1.5 ng/mL. This value is higher than the threshold value fixed by European regulations (50 ng/L in milk). In order to decrease the limit of detection of the sensor, a pre-concentration module is needed. Combining the sensor sensitivity and specificity with a pre-concentration module, the required levels could be accomplished.

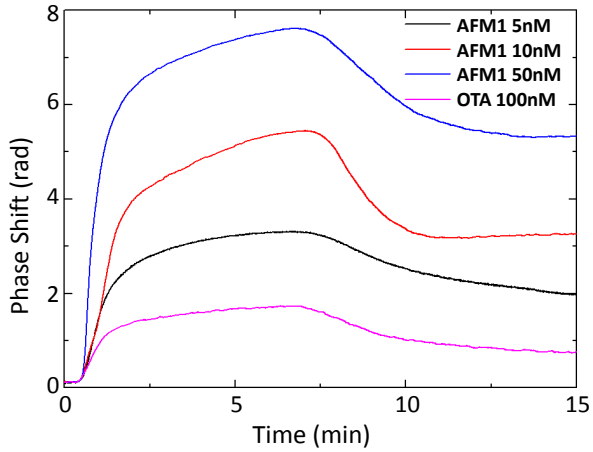

Figure 6. Sensing measurements of 5 nM, 10 nM and 50 nM pure AFM1 and 100 nM OTA diluted in MES performed using four different aMZI based chips functionalized with Fab' strategy. The flowing buffer is MES. Sensorgram shows the phase evolution when the liquid that contains AFM1 at different concentrations flows over the sensors.

To be sure that achieved signals are due to the AFM1 binding, we did measurements to prove the specificity of our sensors. For this purpose we used OTA at 100 nM concentration. Figure 6 shows that even though the concentration of OTA is significantly higher than concentrations of AFM1, the non-specific signal is much lower in comparison with the specific signal. In fact, in the case of AFM1 at 5 nM, after MES rinsing, the phase shift is 2 rad, while for OTA at 100 nM it reaches 0.8 rad.

4. CONCLUSION

In this article, we designed and tested Si_3N_4 biosensors based on asymmetric Mach-Zehnder Interferometers. We achieved a low LOD (LOD $\approx (1.1 \pm 0.2) \times 10^{-6}$) and demonstrated a high selectivity to AFM1 when Fab'-based functionalization is followed by a casein passivation. We obtained a comparative dependence of the phase shift on the concentration of the target toxin. However the measured minimum concentration of AFM1 is still higher than the minimum concentration prescribed by regulations, which indicates the need of a preconcentration module. Other AFM1 sensors have been reported in the literature, which are able to detect AFM1 concentration in the low ppt interval.[12,14] Despite this limitation, the sensor here proposed has the advantage of being compact, easily integrable and scalable to multi-analyte possibility.

We show the specificity of our sensors by comparing the specific and non-specific responses to AFM1 and OTA. Since the measurements we did were on purified samples, further work still needs to be carried out if the sensor should be used with raw milk samples due to the complexity of the milk matrix. Filter and preconcentration stages should be considered to expose the sensor to a purified and concentrated sample extracted from milk.

ACKNOWLEDGMENTS

This work was supported by the FP7 EU project "Symphony" (Grant agreement No: 610580).

REFERENCES

[1] Langmuir, I. and Schaefer, V. J., "Optical measurement of the thickness of a film adsorbed from a solution," *J. Am. Chem. Soc.* **59(7)**, 1406–1406 (1937).

[2] Makarona, E., Petrou, P., Kakabakos, S., Misiakos, K., and Raptis, I., "Point-of-need bioanalytics based on planar optical interferometry," *Biotech. Advances* (2016).

[3] Homola, J., "Surface plasmon resonance sensors for detection of chemical and biological species.," *Chem. Rev.* **108**, 462–493 (2008).

[4] Guider, R., Gandolfi, D., Chalyan, T., Pasquardini, L., Samusenko, A., Pucker, G., Pederzolli, C., and Pavesi, L., "Design and optimization of sion ring resonator-based biosensors for aflatoxin m1 detection," *Sensors* **15**, 17300–17312 (2015).

[5] Heideman, R. G. and Lambeck, P. V., "Remote opto-chemical sensing with extreme sensitivity: design, fabrication and performance of a pigtailed integrated optical phase-modulatedmachzehnder interferometer system," *Sens. Actuator B* **61**, 100–127 (1999).

[6] Chalyan, T., Guider, R., Pasquardini, L., Zanetti, M., Falke, F., Schreuder, E., Heideman, R. G., Pederzolli, C., and Pavesi, L., "Asymmetric mach-zehnder interferometer based biosensors for aflatoxin m1 detection," *Biosensors* **6(1)**, 1 (2016).

[7] Samusenko, A., Gandolfi, D., Pucker, G., Chalyan, T., Guider, R., Ghulinyan, M., and Pavesi, L., "A sion microring resonator-based platform for biosensing at 850 nm," *IEEE J. of Lightw. Tech.* (2016).

[8] Heideman, R., Hoekman, M., and E, S., "Triplex-based integrated optical ring resonators for lab-on-a-chip and environmental detection," *IEEE J. Sel. Top. Quantum Electron.* **18**, 1583–1596 (2012).

[9] Crivianu-Gaita, V. and Thompson, M., "Immobilization of fab1 fragments onto substrate surfaces: A survey of methods and applications," *Biosens. Bioelectron.* **70**, 167180 (2015).

[10] K, W., Heideman, R., Leinse, A., and Hoekman, M., "Triplex: A versatile dielectric photonic platform," *Adv. Opt. Technol.* **4**, 189–207 (2015).

[11] Gandolfi, D., [*On-chip photonic label-free biosensors*], PhD Thesis, University of Trento,Trento, Italy (2015).

[12] Brosinger, F., Freimuth, H., Lacher, M., Ehrfeld, W., Gedig, E., Katerkamp, A., Spener, F., and Cammann, K. A., "Label-free affinity sensor with compensation of unspecific protein interaction by a highly sensitive integrated optical machzehnder interferometer on silicon," *Sens. Actuators B Chem.* **44**, 350–355 (1997).

[13] Yoshimoto, K., Nishio, M., Sugasawa, H., and Nagasaki, Y., "Direct observation of adsorption-induced inactivation of antibody fragments surrounded by mixed-peg layer on a gold surface.," *J. Am. Chem. Soc.* **132**, 79827989 (2010).

[14] Liu, Q., Tu, X., Kim, K. W., Kee, J., Shin, Y., Han, K., Yoon, Y. J., Lo, G. Q., and Park, M. K., "Highly sensitive machzehnder interferometer biosensor based on silicon nitride slot waveguide," *Sens. Actuators B Chem.* **188**, 681–688 (2013).